VILNIAUS GEDIMINO TECHNIKOS UNIVERSITETAS

STATYBOS FAKULTETAS

METALINIŲ IR KOMPOZITINIŲ KONSTRUKCIJŲ KATEDRA

Tautvydas Zakaras

Aliumininių profiliuočių lokalaus stabilumo tyrimai

Investigating local stability of aluminium profiles

Baigiamasis magistro darbas

Statinių konstrukcijų studijų programa, valstybinis kodas 6211EX040

Lengvosios šiuolaikinės konstrukcijos specializacija

Statybos inžinerija 02T mokslo kryptis

Vilnius, 2021

VILNIAUS GEDIMINO TECHNIKOS UNIVERSITETAS
STATYBOS FAKULTETAS
METALINIŲ IR KOMPOZITINIŲ KONSTRUKCIJŲ KATEDRA

TVIRTINU
Katedros vedėjas

(Parašas)
Antanas Šapalas
(Vardas, pavardė)

(Data)

Tautvydas Zakaras

Aliumininių profiliuočių lokalaus stabilumo tyrimai

Investigating local stability of aluminium profiles

Baigiamasis magistro darbas

Statinių konstrukcijų studijų programa, valstybinis kodas 6211EX040,
Lengvosios šiuolaikinės konstrukcijos specializacija
Statybos inžinerija 02T studijų kryptis

Vadovas	dr. Viktor Gribniak (Moksl. laipsnis/pedag. vardas, vardas, pavardė)	(Parašas)	2021-06-03 (Data)
Konsultantas	(Moksl. laipsnis/pedag. vardas, vardas, pavardė)	(Parašas)	(Data)
Konsultantas	(Moksl. laipsnis/pedag. vardas, vardas, pavardė)	(Parašas)	(Data)

Vilnius, 2021

VILNIUS GEDIMINAS TECHNICAL UNIVERSITY
FACULTY OF CIVIL ENGINEERING
DEPARTMENT OF STEEL AND COMPOSITE STRUCTURES

Civil Engineering field

Structural Engineering study programme, state code 6211EX040

Lightweight Modern Structures specialization

APPROVED BY
Head of Department

(signature)
prof. dr. Antanas Šapalas
(Name, Surname)

(date)

OBJECTIVES FOR MASTER THESIS
2020-02-03 No. 01
Vilnius

For student Tautvydas Zakaras

Master Thesis title: Investigating local stability of aluminium profiles

Approved on 9 March 2021 by Dean's decree No. 80st
(day, Month, year)

The Final work has to be completed by 30 May 2021.
(day, Month, year)

THE OBJECTIVES:

The deformation behaviour and local stability of aluminium profiles (mullions) is the research object of this MSc Thesis. The idea of this research is related to the possibility of improving the profiles' local stability by applying low-modulus polymer stiffeners. The study also investigates the efficiency of strengthening techniques typical for the facade building industry expressed in terms of ultimate load-carrying capacity and weight ratio. The above problems must employ a reliable numerical model of the composite profile with polymeric stiffeners verified using the corresponding physical tests' results.

Academic Supervisor .... Dr Viktor Gribniak
(signature) (Title, Name, Surname)

Objectives accepted as a guidance for my Master Thesis

....
(Student's signature)

Tautvydas Zakaras
(Student's Name, Surname)
2020-02-03
(Date)

Vilniaus Gedimino technikos universiteto egzaminų sesijų ir baigiamųjų darbų rengimo bei gynimo organizavimo tvarkos aprašo
2 priedas

(Baigiamojo darbo sąžiningumo deklaracijos forma)

VILNIAUS GEDIMINO TECHNIKOS UNIVERSITETAS

Tautvydas Zakaras, 20152336

(Studento vardas ir pavardė, studento pažymėjimo Nr.)

Statybos fakultetas

(Fakultetas)

Statinių konstrukcijos, LŠKfm-19

(Studijų programa, akademinė grupė)

BAIGIAMOJO DARBO (PROJEKTO)

SĄŽININGUMO DEKLARACIJA

2021 m. birželio 02 d.

Patvirtinu, kad mano baigiamasis darbas tema „Aliumininio profiliuočio lenkiamojo standumo didinimo galimybių tyrimas" patvirtintas 2021 m. kovo 09 d. dekano potvarkiu Nr. 80st, yra savarankiškai parašytas. Šiame darbe pateikta medžiaga nėra plagijuota. Tiesiogiai ar netiesiogiai panaudotos kitų šaltinių citatos pažymėtos literatūros nuorodose.

Mano darbo vadovas daktaras Viktor Gribniak.

Kitų asmenų indėlio į parengtą baigiamąjį darbą nėra. Jokių įstatymų nenumatytų piniginių sumų už šį darbą niekam nesu mokėjęs (-usi).

(Parašas)

Tautvydas Zakaras

(Vardas ir pavardė)

Vilniaus Gedimino technikos universitetas
Statybos fakultetas
Metalinių ir kompozitinių konstrukcijų katedra

ISBN ISSN
Egz. sk. ....
Data ..........-.....-.....

Antrosios pakopos studijų **Statinių konstrukcijų** programos magistro baigiamasis darbas

Pavadinimas **Aliumininio profiliuočio lenkiamojo standumo didinimo galimybių tyrimas**

Autorius **Tautvydas Zakaras**

Vadovas **Viktor Gribniak**

Kalba: anglų

Anotacija

Magistro baigiamajame darbe nagrinėjamas aliumininių profiliuočių lokalus stabilumas. Tiriamąjį darbą sudaro keturi skyriai. Pirmajame skyriuje aptariama naudojamų aliumininių profiliuočių galimybės, jų stiprinimo galimybės su kompozitinėmis medžiagomis, šių medžiagų efektyvumas. Antrajame skyriuje skyriuje atlikti šešių taškų lenkimo bandymai su tipiniais profiliuočių stiprinimo būdais fasadų industrijoje. Efektyviausias stiprinimo būdas nustatomas pagal laikomosios galios ir savojo svorio santykį. Trečiajame skyriuje atlikti tempimo bandymai aliuminio mechaninėms savybėms nustatyti, gniuždymo bandymai- plastikinių sąstandų mechaninėms savybėms nustatyti. Taip pat atlikti trijų taškų lenkimo bandymai su lokaliai sustandintais profiliuočiais. Ketvirtame skyriuje pateiktas sumodeliuotas skaitinis modelis siekiant atkartoti eksperimentų rezultatus. Remiantis atlikta literatūros analize, eksperimentais ir skaitiniu modeliu pateikiamos išvados ir pasiūlymai. Darbą sudaro 45 puslapiai, 26 paveikslai, 2 lentelės ir 50 literatūros šaltinių.

Prasminiai žodžiai: Aliumininiai profiliuočiai, plastikinės sąstandos, stiprinimas, fasadai, lenkimo bandymai, skaitinis modeliavimas.

Vilnius Gediminas Technical University
Faculty of Civil Engineering
Department of Steel and Composite Structures

ISBN ISSN
Copies No. ....
Date ..........-.....-.....

Master Degree Studies **Structural Engineering** study programme Master Graduation Thesis

Title	**Analysis of possibilities for increasing bending stiffness of aluminum profile**
Author	**Tautvydas Zakaras**
Academic supervisor	**Viktor Gribniak**

Thesis language: English

Annotation

The local stability of aluminum profiles is investigated in this Master's Thesis. The research work consists of four sections. The first section discusses the possibilities of used aluminum profiles, their strengthening possibilities with composite materials and the efficiency of those materials. In the second chapter, six-point bending tests are performed with typical profile strengthening techniques for the facade building industry. The most effective method of reinforcement is determined by the ratio of load bearing capacity to dead weight. In the third chapter, tensile tests were performed to determine the mechanical properties of aluminum, compression tests were performed to determine the mechanical properties of plastic stiffeners. Three-point bending tests with locally stiffened profiles were also performed. The fourth section presents a simulated numerical model to replicate the experimental results. Based on the performed literature analysis, experiments and numerical model, conclusions and suggestions are presented. Master's Thesis consists of 45 pages, 26 figures, 2 tables and 50 literature references.

Keywords: Aluminum profiles, plastic stiffeners, strengthening, facades, bending tests, numerical analysis.

Table of Content

List of Figures

List of Tables

General Work Characteristic

The external walls are an integral part of the building. In most cases, masonry walls held loads and transferred them to other building structures, but with the development of construction technologies, both steel and reinforced concrete columns emerged, which perfectly changed the design concept. As a result, restrictions on the facade of the building have been reduced and more architectural expressiveness has emerged. Since the main function of the facade is to protect the building from the effects of the atmosphere and ensure good acoustic insulation, the external walls can be installed from lightweight structures. One of the most widely used construction materials today is glass and aluminum. Aluminum was first invented in 1825. The strength of pure aluminum is 90 MPa. Due to the low strength, it took many years for aluminum to be used in construction. Many studies and experiments have been carried out with various aluminum alloys and today some of them keep one‘s end up with the strength of steel. One of the most popular aluminum alloy EN AW-7020 has a yield strength of 280 MPa and corresponds to steel class S275. Around the 1970s, with the popularity of aluminum extrusion, aluminum began to be used for facade glazing. Today, very tall buildings are being built in the world, and aluminum-glass constructions are most often chosen for the facade. The main load that the facade has to withstand is wind. The tops of tall or seafront buildings are subject to very high wind loads. However, the hollow aluminum profile usually does not have sufficient bending stiffness, so it has to be reinforced with additional inserts.

Problem Formulation

In high-rise buildings, using aluminum profiles as a façade structure, high wind loads and formations prevail on the upper floors, which can cause profile deformations to exceed limit values, and support unit structures can cause stress concentrations and thus endanger building operation. Therefore, it is necessary to study the bending stiffness of reinforced profiles with already used reinforcement methods and to test new reinforcement methods with embedded plastic stiffeners.

Relevance of Work

Aluminum constructions are often used in facades because it reduces the cost of construction and gives more freedom in choosing the look of the building. There have been a number of studies with reinforcements of various metal profiles with various details or materials, but there are almost no experiments with reinforcement of aluminum. Determining the most effective method of reinforcement could increase the reliability of buildings.

The Object of the Research

The object of research in this MSc Thesis is aluminum profiles. The aim is to examine the possibilities of increasing their flexural stiffness and local stability.

Work Objective

The aim of the MSc Thesis is to experimentally determine the bending stiffness of aluminum profiles and find an optimal way to strengthen them and increase local stability.

Main Tasks of Work

To achieve the goal of the work, the following tasks are set:

1. To carry out literature analysis on strengthening of aluminum profiles.
2. To perform six-point bending tests to determine the efficiency of strengthening techniques typical for facade building industry.
3. To produce (print with a 3D printer) polymer stiffeners of various densities and to strengthen aluminum profiles accordingly.
4. To perform three-point bending and compressive tests of aluminum profiles strengthened with polymeric stiffeners.
5. To determine the mechanical properties of aluminum profile and polymeric stiffeners.
6. To create a computer model representing local buckling of the tested aluminum samples.
7. To evaluate the possibilities of strengthening aluminum profiles with low-modulus printed stiffeners.

Methods of the Research

The investigation employs the literature analysis, mechanical tests in the laboratory, statistical analysis of the test results, and numerical modelling with finite element software.

Acknowledgement

The Author want to express his sincere gratitude to the Colleagues from the Laboratory of Innovative Building Structures dr. Ieva Misiūnaitė, dr. Arvydas Rimkus, and dr. Aleksandr Sokolov for assistance in providing experimental investigation and second-order elastic analysis.

1. Literature Review

Facades of modern, high-rise buildings are the frequent objects of application aluminium profiles (Sivaprakasam et al., 2020). Reduction of the self-weight governs the development of these structural shapes (Lee et al., 2017): decrease of the web thickness together with an increase of the profile height ensures the required flexural resistance of the building components. However, the cost reduction of the facade systems is not a single optimisation criterion (Lesniak et al., 2020). The investigation by Lee *et al*. (2018) demonstrated that the optimum thickness of the web could reach 1 mm, but that makes such elements vulnerable to web crippling. This form of localised buckling occurs due to the stress concentration in the load application zones and supports of structural members. Similar effects are also characteristic of the application of the high-strength steel tubular elements (Misiunaite et al., 2020).

The web crippling of thin-walled aluminium and cold-formed steel element is a typical failure mode. It has been investigated thoughtfully (Wang et al., 2016; Chen et al., 2015; Zhou and Young, 2008). Local strengthening is a possible solution to the buckling problem. External and internal strengthening systems have been developed to avoid the web crippling. The external strengthening refers to supplementary plates connected to the web, smoothing the stress concentrations (Zhao and Zhang, 2007). The internal systems employ various fillers and plugs; this solution is typical for laboratory tests of hollow section profiles and the development of structural composites (Misiunaite et al., 2020; Wang et al., 2016; Bock et al., 2021).

Recently, polymeric materials become a promising solution to improve the buckling performance of metallic structures (Zhao et al., 2007; Fernando et al., 2009; Schnerch, 2005; Islam and Young, 2011; Islam and Young, 2012; Islam and Young, 2018; Wu et al., 2011). An adhesive connection typically forms such composite structures and governs the effectiveness of the strengthening systems (Fernando et al., 2009). Thus, the debonding failure is a critical issue for the strengthening of metallic components (Zhao et al., 2007; Fernando et al., 2009; Schnerch, 2005; Islam and Young, 2011; Islam and Young, 2012). Commonly, this failure localises within the adhesive layer (cohesion failure) or at the physical interface of the adherents (adhesion failure) (Zhao et al., 2007; Schnerch et al., 2005). Mechanical properties of the adhesive control the cohesion failure. Still, the adhesion failure depends on the contact characteristics of the adherents, including the texture, roughness and chemical composition of the surface (Schnerch et al., 2005).

Local stability of aluminium profiles (mullions) is the focus of this research. Remarkably, the adhesive bonding behaviour of carbon steel and aluminium is different. It is a consequence of the differences in the stress-strain response of these materials: the aluminium products have lower elasticity modulus and proportional limit than carbon steel elements. That affects the premature buckling and web crippling of the structural members. Consequently, adhesion failure becomes the typical debonding failure of the aluminium-based structural composites (Islam and Young, 2011; Islam and Young, 2012).

The studies (Lee et al., 2018; Sewell et al., 2016) related the solution of the buckling problem to the production of composite mullions comprising low-modulus filler material to stabilise the deformations of the web. The deformation behaviour of infilled tubular profile having thin webs is quite similar to sandwich composite under edgewise loading. The analysis of sandwich components (Eyvazian et al., 2019; Taghizadeh et al., 2019) demonstrated the structural efficiency of the above solution: the substantial increase in both load-bearing capacity and the absorption of the deformation energy was the consequence of the tests of the composite systems.

The recent studies reported in the literature demonstrated that the strength and stiffness of the core material affect the load-bearing capacity of sandwich structures, especially under an edgewise compressive load (Eyvazian et al., 2019; Mamalis et al., 2005; Hongshuai et al., 2016). A low-density honeycomb core provides excellent structural stability (Djama et al., 2019). Aluminium foam (Xiao et al., 2018), polyurethane foam (Waddar et al., 2019), and NOMEX paper honeycombs (Zhang et al., 2018) were efficiently used as sandwich cores. However, traditional thermosets and metallic mixes formed all sandwich structures mentioned above. Thus, the utilisation of these structures faces severe recycling problems (Chen et al., 2019; Shi et al., 2019). Recyclable thermoplastic materials become considerably advertised in advanced engineering applications to overcome this problem (Schneider et al., 2015; Gao et al., 2020). The thermoplastic composites are gaining in recognition due to inherent advantages of thermoplastics, such as thermoformability which results in manufacturing process innovations that deliver on cost efficiency (Sewell et al., 2016; Das et al., 2020).

Among various technologies used for the production of the core material of sandwich composites, additive manufacturing has been frequently investigated because of the distinguished advantages of mass customisation and ability to manufacture complex structures (Hou et al., 2018; Sarvestani et al., 2018; Ngo et al., 2018; Zaharia et al., 2020). Studies by Lu et al. (2018) and Li & Wang (2017) highlighted the suitability of the architected core structures to tailor the bending properties and failure mechanisms of sandwich structures. Lubombo & Huneault (2018) investigated the stiffness and strength of cellular 3D-printed parts under uniaxial tensile and flexural loading. The cellular components were fabricated using various types of infill patterns at different infill density levels. The stiffness and strength scaled with the infill density. Besides, at the same printing density, the mechanical response varied substantially, depending on the infill patterns and the number of perimeter shells. Bates *et al*. (2016) concluded that optimised topology of the 3D-printed core ensures enhancing the energy absorption abilities of the honeycomb structures. The strain rate and cell orientation to the compression direction affected the absorption capacity.

The above studies demonstrated the potential of additive manufacturing technologies for the creation and optimisation of core element topologies, which are not constrained by traditional manufacturing principles, offering the designer the capability to create resilient sandwich structures tailored explicitly to operational applications. Moreover, the computer-based additive manufacturing principles fit the Industry 4.0 concept that relates the revolutionary development of the technology to the manufacturing robots and humans interaction (Cerutti et al., 2019). However, 3D-printed prototypes can inadequately replicate the mechanical behaviour of real objects (Alhammer et al., 2020). Therefore, the structural application of printed materials requires characterisations.

This study consists of two parts. At the first stage, the efficiency of the industrial strengthening techniques is estimated. Several full-scale hollow section aluminium profiles (mullions) available on the market were tested simulating uniformly distributed flexural load. The ultimate bending load and the unit weight ratio determines the strengthening efficiency. The failure mechanism is also investigated. This study illustrates the essential role of local profile resistance to mechanical load. That is characteristic of structural connections of the facades.

Therefore, the second part of this MSc Thesis aims to demonstrate the development feasibility of efficient composite systems comprising aluminium profiles and low-modulus polymeric stiffeners. The hollow section aluminium profile tested at the first investigation stage was the subject of the six-point bending test simulating distributed load. The buckling failure was the testing result of the samples. Polymer stiffeners produced using a 3D printing technique strengthened alternative samples for the comparison purpose. The printing density of the stiffeners was the variable of this study. The previous material tests (Gribniak et al., 2019; Shkundalova et al., 2018) determined the design of the stiffeners. A 10% infill density of the polymer was the minimum value used in this investigation. Numerical simulations are carried out to analyse nonlinear effects characteristic of the deformation behaviour of the profiles.

2. Full-Scale Profile Tests

2.1 Test Specimens

The tests were carried out in the Laboratory of Innovative Building Structures at Vilnius Tech. The 2 m long mullions were tested to investigate the efficiency of strengthening techniques typical for facade building industry. A six-point-bending test simulated the uniformly distributed load the facade structure. Three types of strengthened specimens were fabricated, producing two identical samples of each specimen types. Thus, six profiles were tested in total. Figure 1 depicts cross-section of the specimens. Figure 1b shows a special extruded profile fixed with self-drilling screws to the mullion. Screws were placed at 10 cm from both ends with a step of 30 cm. In Figure 1c, two zinc coated metal sheets connected to a mullion with self-tapping screws strengthen the aluminium profile. Hereafter, these specimen types are designated as to Type A, Type B, and Type C. The distances between screws are the same as in specimen shown in Figure 1b. Figure 1d shows the mullion with inserted flat steel bars and extruded aluminium profile. The 10 mm bolts, placed 10 cm from both ends of the sample, connect the structural components.

2.2 Flexural tests: Six-Point Bending

The reduction of the self-weight of facade structures determines the main benefit of aluminium profiles. However, strengthening reduces the profile efficiency by increasing the profile weight. For example, a unite aluminium profile meter weight is equal to 3.050 kg; the respective parameter of the profiles shown in Figure 1b-Figure 1d are 5.852 kg, 9.272 kg, and 15.037 kg that is 1.92, 3.04 and 4.93 times heavier than an empty profile. That shows the limited strengthening ability of improving the structural performance of aluminium facades. Therefore, the ultimate bending load and the unit weight ratio of the strengthened profiles is the research object of this Section.

The flexural tests were carried out using an electromechanical machine *w+b LFV 5000* with a loading capacity of 100 kN, under displacement control with a loading rate of 0.042 mm/s. Deformations of six specimens were monitored using a digital image correlation (DIC) technique. The spray paint was utilised to apply a high-contrast random pattern to the monitoring surface (Figure 9b). A digital single-lens reflex camera *Canon EOS 77D SLR* with 18-135 mm *Canon EF-S* lens placed on a tripod at a 0.4 m distance from the monitored surface captured the digital images. The 6000×4000 pixel images were captured at the load increments of 0.5 kN using following settings of the camera: exposure time = 1/200 s, aperture = f/4.5, sensitivity to light = ISO 100, focal length =

24 mm. A remote control device was used to avoid unexpected movements of the camera. A 100 kN load-cell monitored the applied load. The LVDT devices were placed as shown in Figure 1a.

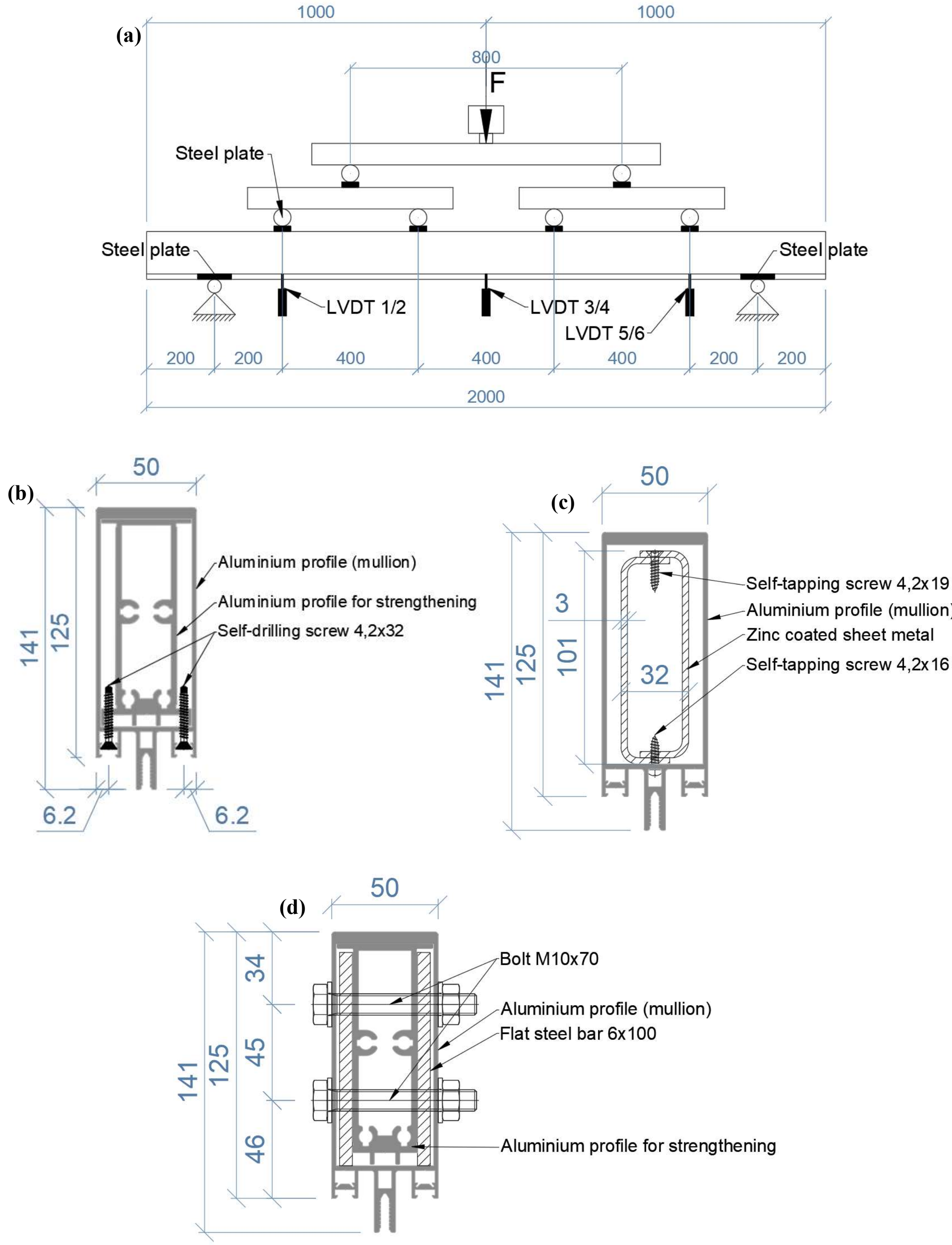

Figure 1. Six-point bending test (units [mm]): (a) loading scheme; (b) cross-section strengthened with aluminium profile (Type A sample); (c) cross-section strengthened zinc coated metal sheets (Type B); (d) cross-section strengthened with aluminium profile and flat steel sheets (Type C).

Figure 2 shows the experimental setup and load-vertical displacement diagrams measured at the mid-span of the profiles. Figure 3 shows the failure mechanism of the test specimens.The load-displacement diagrams (Figure 2b) show that Type A and Type B demonstrated almost identical load-bearing capacity, though the profiles strengthened with aluminium profiles (Type A) possessed a more ductile failure than Type B counterparts. On the contrary, Type C samples experienced 1.75 times higher ultimate load than the above mentioned samples. Note, the specimen C-1 demonstrated slightly different ultimate behaviour (regarding the sample C-2) because of unexpected rotation of the testing apparatus supports (Fig. 3c). Thus, this specimen was excluded from the further analysis. Larger load-bearing capacity than the other two types of profiles; the increase in deformations corresponding to the ultimate resistance was 1.12 and 1.48 times in mullions with extruded strengthening profile and zinc coated sheet metals, respectively.

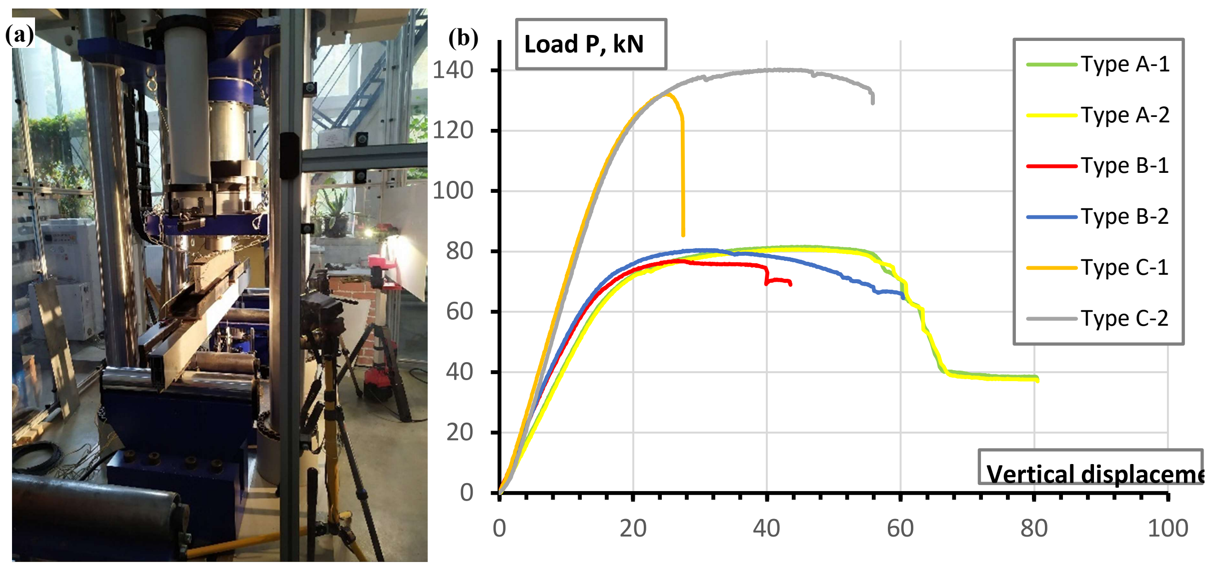

Figure 2. Six-point bending test: (a) test apparatus; (b) load-vertical displacement diagrams of all specimens.

Figure 3. Deformed shape of the flexural elements: (a) Type A; (b) Type B; (c) Type C.

Figure 4. Local buckling of specimen Type A.

Table 1. Ultimate load and displacement values of six-point bending specimens

No	Specimen	Ultimate Load, kN	Displacement, mm	Failure mechanism	Ultimate load/unite meter weight ratio
1.	Type A-1	81.6	41	Local buckling	13.94
2.	Type A-2	80.6	41	Local buckling	13.77
3.	Type B-1	76.9	27	Local buckling	8.29
4.	Type B-2	80.4	31	Local buckling	8.67
5.	Type C-1	132.3[1]	25	Out of plane	8.8
6.	Type C-2	140.3	46	Local buckling	9.33

[1] Unexpected rotation of the testing apparatus supports caused a different result. Thus this specimen is excluded from analysis

Table 1 demonstrates that the strengthening technology when the additional aluminium profiles inserted inside the mullions (the specimens Type A is the most efficient way for improving the ultimate behaviour of aluminium facade bending elements. Ultimate load to unite meter weight ratio is 1.63 and 1.53 times higher than Type B and Type C specimens respectively are. The breakage of the aluminium bottom part caused the failure of the strengthened profiles. Figure 3 shows the deformed shape of the bending specimens. Thus, the profiles faced premature loss of flexural stiffness. However, a local buckling was the consequence of the bending tests of the specimens Type A, inducing the plastic plateau (Figure 4). With the ultimate bending load and the unit weight ratio of the strengthened profiles being the main object of this section, Type A specimens were the most effective ones. Thus, the next section investigates the development feasibility of efficient composite systems comprising aluminium profiles and low-modulus polymeric stiffeners, avoiding premature loss of the deformation resistance.

3. Local Buckling Analysis

3.1 Test Specimens

A three-point bending test determined the deformation behaviour of an aluminium profile. A hollow section profile, made from aluminium EN AW 6060 T66, available on the market was the test subject. Figure 5a shows the loading scheme of three-point bending. Figure 5b depicts the cross-sections of the three-point bending specimen.

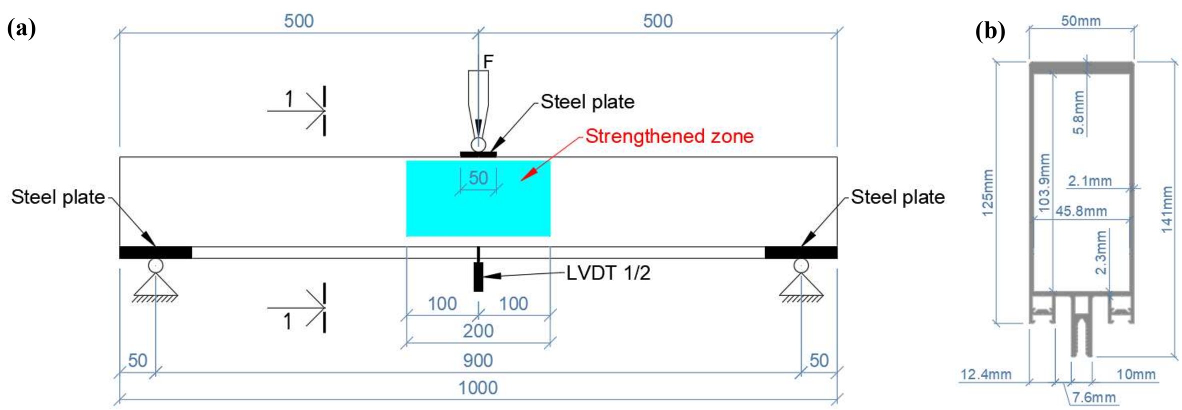

Figure 5. Three-point bending test (units [mm]): (a) loading scheme; (b) cross-section of the profile.

The reference 1 meter specimens had no additional stiffeners. On the contrary, polymer stiffeners strengthened alternative samples. A sky-blue shading indicates the stiffened zone in Figure 5a. The stiffeners were produced using a 3D printing technique. They had the dimensions corresponding to the internal shape of the profile (Figure 5b) and 10 mm thickness; thus, 20 segments, glued together with epoxy adhesive, strengthened each alternative profile.

A 3D printed thermoplastic polymeric material was used producing the stiffeners. A low deformation modulus of the polymeric material can reduce local stress concentrations due to high deformability of the material (Gribniak et al., 2019). Shkundalova *et al*. (2018) investigated the mechanical properties and tensile failure of four thermoplastic polymeric materials: acrylonitrile butadiene styrene (ABS), polylactic acid (PLA), high impact polystyrene (HIPS), and polyethylene terephthalate (PETG). The investigation shown that the ultimate strain of the specimens made of ABS, HIPS and PETG localised between the printed filaments causing local brittle failure of the tensile specimen. On the contrary, the PLA experienced a ductile failure providing the highest nominal tensile strength (37.7 MPa) of the material. Thus, the 3D printing employed PLA.

Figure 6 shows the printer, the stiffeners having different infill, and the strengthening procedure. The stiffeners were printed using PRUSA i3 MK3 printer (Figure 6a) with identical printing parameters: extrusion nozzle temperature = 215°C; printing bed temperature = 60° C; print speed = 28 mm/s. The 1.75 mm PLA filament *Prusament* having 1240 kg/m^3 density was used.

The stiffeners were printed in the horizontal position; the thickness of each printing layer was 0.2 mm. Two continuous "shells" having the 100% density were printed on the perimeter of each specimen. The inner part of the samples was printed at rectilinear raster orientation inclined at 45°. Such a printing layout is frequent for the prototyping. The infill density was the variable of this study.

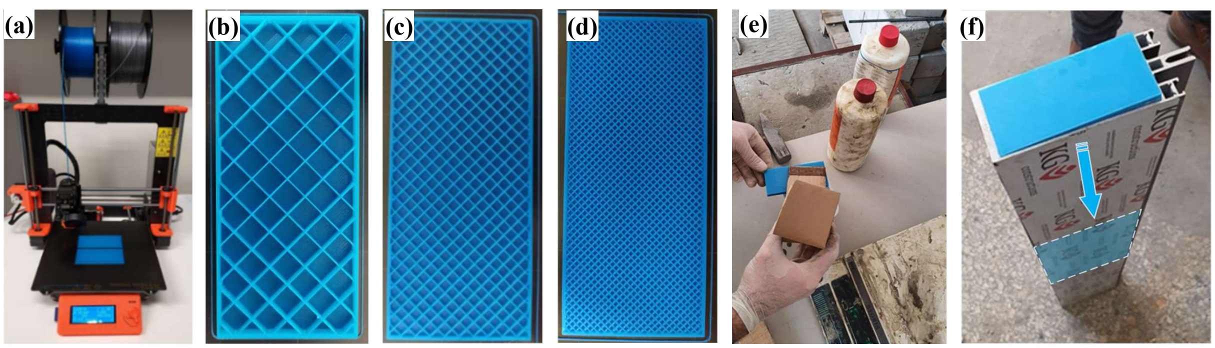

Figure 6. Strengthening procedure: (a) PRUSA i3MK3 printer; (b), (c), and (d) printed stiffeners having 10%, 25%, and 50% density of the infill; (e) and (f) a stiffener segment coated with epoxy adhesive before and after inserting it inside the aluminium profile

This MSc Thesis reports results of 3 series of the specimens having 10%, 25%, and 50% infill density of the printed stiffeners (Figure 6b-Figure 6d). As it can be observed in Figure 6e, a two-component adhesive (*Epoxydharz L* resin and *Härtel L* hardener) was used to fix the stiffeners inside the profile (Figure 6f). Eight specimens were produced to analyse local deformations of the strengthened profile fragments under compression. The length of the samples was equal to 50 mm. The segments were cut from the flexural profiles and had the same cross-section (Figure 5b). The bottom surface was levelled to avoid stress concentration. Four 10 mm thickness stiffeners (identical to the ones used for the flexural tests) were inserted in the centre part of the strengthened samples. The same adhesive fixing the plastic details and printing density of the stiffeners, as in the flexural specimens, were used. Two items of each type were produced, as shown in Figure 7. Two additional samples were produced to investigate the adhesion effect between the stiffeners and profile on the local deformations under compression. One of them had no adhesive fixation of the stiffener with profile; another was the bare stiffener. Both stiffeners had a 10% infill density.

Twelve tensile samples were also tested to determine the mechanical properties of aluminium: equal number (six) of specimens were cut from 5.8 mm flange and 2.1 mm web (Figure 5b). The test samples were designated correspondingly as to F-5.8 and W-2.1. Figure 8 shows the dimensions of the tensile specimens.

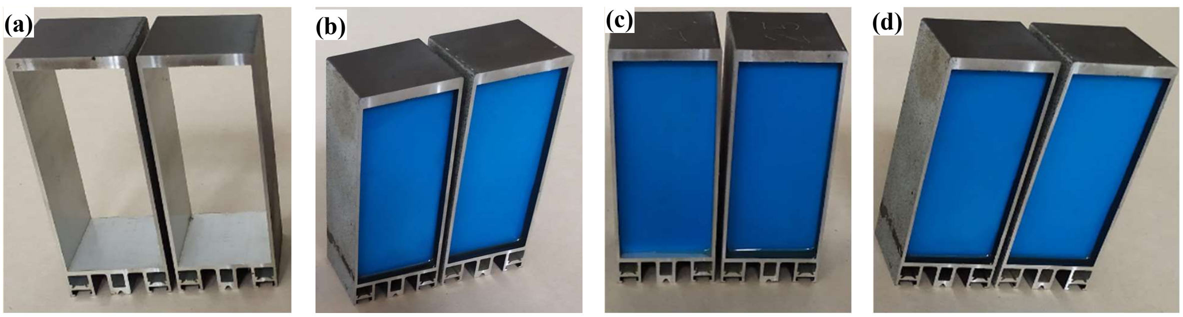

Figure 7. Specimens for compressive tests: (a) reference samples, (b), (c), and (d) the specimens strengthened with stiffeners having 10%, 25%, and 50% infill density, respectively.

(a)

(b)

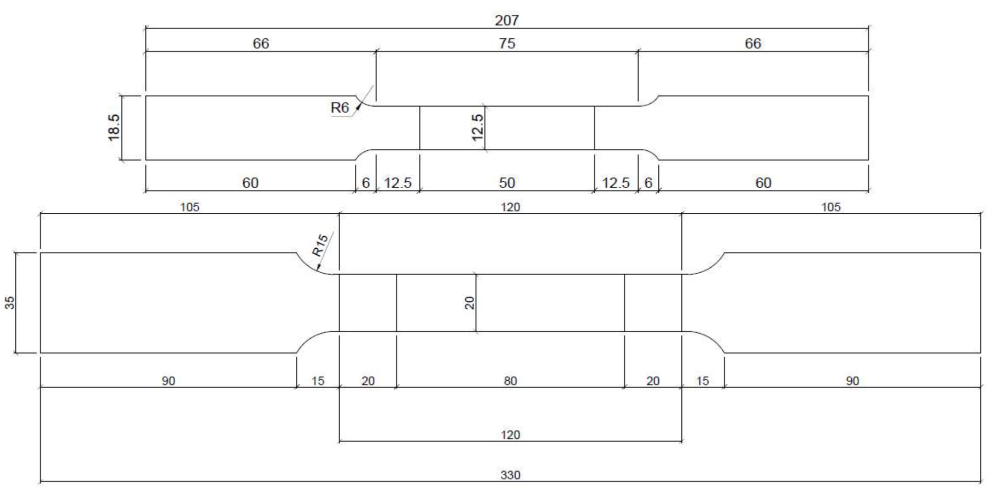

Figure 8. Tensile samples (dimensions in mm): (a) specimen W-2.1 cut from 2.1 mm web; (b) specimen F-5.8 cut from 5.8 mm flange.

3.2 Tensile Tests

The tests were carried out using the 200 kN tensile machine *P-20* with loading rate of 100 N/s. Figure 9 illustrates the tensile tests. The same DIC system, as described in the section “Flexural tests. Six-point bending”, monitored the relative displacements of the specimens. The relative strain distribution maps were determined by using *GOM Correlate* software. Figure 9c shows an example of the deformation monitoring results. The uniform distribution of the strains is characteristic of the tensile sample until the failure.

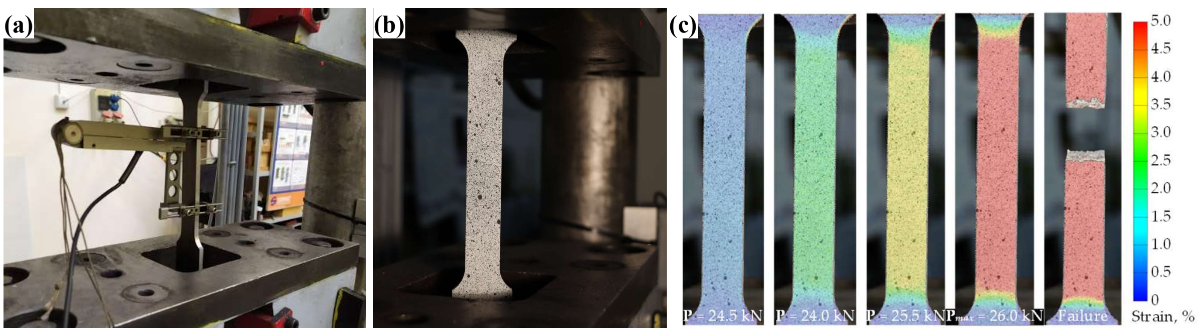

Figure 9. Tensile tests: (a) specimen equipped with an extensometer; (b) sample prepared for DIC measurements; (c) strain distribution of sample F-5.8 captured by the DIC system.

The extensometer *MFA 25-12* (Figure 9a) measured deformations of the remaining eight samples. The measurement base of the specimens W-2.1 (Figure 8a) and F-5.8 (Figure 8b) was equal to 50 mm and 80 mm, respectively. A grip failure caused the loss of the experimental data of one sample W-2.1. Figure 10 shows the stress-strain diagrams estimated from the tensile tests.

Table 2 specifies the determined mechanical parameters of the aluminium samples, including 0.2% proof strength (f_0), ultimate tensile strength (f_u), elongation percentage after fracture (A), and the elastic modulus (E). The table also includes the strength ratio (f_u/f_0). A perfect agreement between test data of the specimens W-2.1 and F-5.8 is characteristic of ultimate strength f_u. The corresponding average difference between the results is equal to 0.1%. The differences in the yielding limit f_0 and the elastic modulus increase to 2.0% and 10.3%, respectively. The later difference demonstrates the potential vulnerability of the thin web to deformation localisation. This difference is also significant for numerical analysis (Misiunaite et al., 2020).

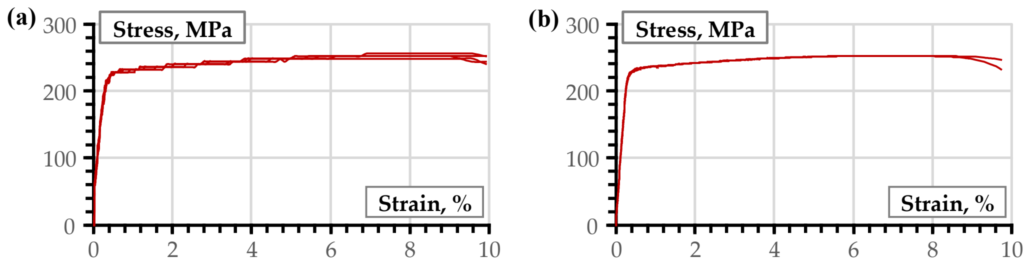

Figure 10. Stress-strain diagrams of aluminium: (a) specimens W-2.1; (b) specimens F-5.8.

Table 2. Mechanical properties of tensile aluminium samples.

No	Specimen	E, GPa	f_0, MPa	f_u, MPa	A, %	f_u/f_0
1.	W-2.1	66.0	228	248	9.60	1.09
2.	W-2.1	70.4	228	256	9.85	1.12
3.	W-2.1	– [1]	228	252	9.50	1.11
4.	W-2.1	71.7	228	252	10.1	1.10
5.	W-2.1	73.6	228	252	9.18	1.11
6.	F-5.8	78.6	233	252	11.3	1.08
7.	F-5.8	78.4	232	253	10.4	1.09

[1] A substantial scatter of the test results did not allow achieving acceptable correlation value.

3.3 Compressive Tests

The compressive tests were carried out using an electromechanical machine *H75KS* (*Tinius Olsen*, Norway) with a loading capacity of 75 kN, under displacement control with a loading rate of 0.25 mm/min. Linear variable displacement transducers (LVDT) with 0.001 mm precision measured the vertical displacements; a 50 kN load-cell measured the applied load. The specimens were tested until the failure. Figure 11 shows the test setup.

The same DIC system, as described in the section "Flexural tests. Six-point bending", monitored the relative displacements of the specimens. The difference was that two identical digital cameras *Canon EOS 77D SLR* monitored opposite side surfaces of the compressive cross-section fragments (Figure 7). The cameras were placed at 0.4 m distance from the monitoring surface; the digital images were captured every 0.5 kN.

Figure 12 shows the final deformed shapes of all compressive specimens. The asymmetric failure shape is characteristic of the reference specimens (Figure 12b). The stiffeners make the deformed shape symmetrical, changing the load resistance mechanisms. Figure 13 shows an example of a deformation evolution identified by the DIC system. The images are related to vertical displacement u of the compression support of the testing machine. The stiffeners compensated the unsymmetrical loss of the adhesive contact with the web (see the second image in the line). At advanced loading stages, the deformation localisation follows the printing layout (Figure 6b).

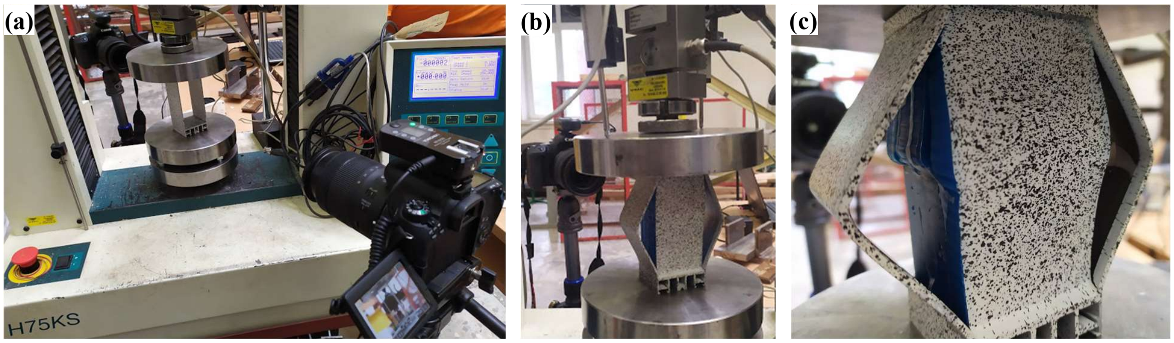

Figure 11. Compressive tests: (a) test apparatus; (b) strengthened sample; (c) a typical failure of the strengthened specimen.

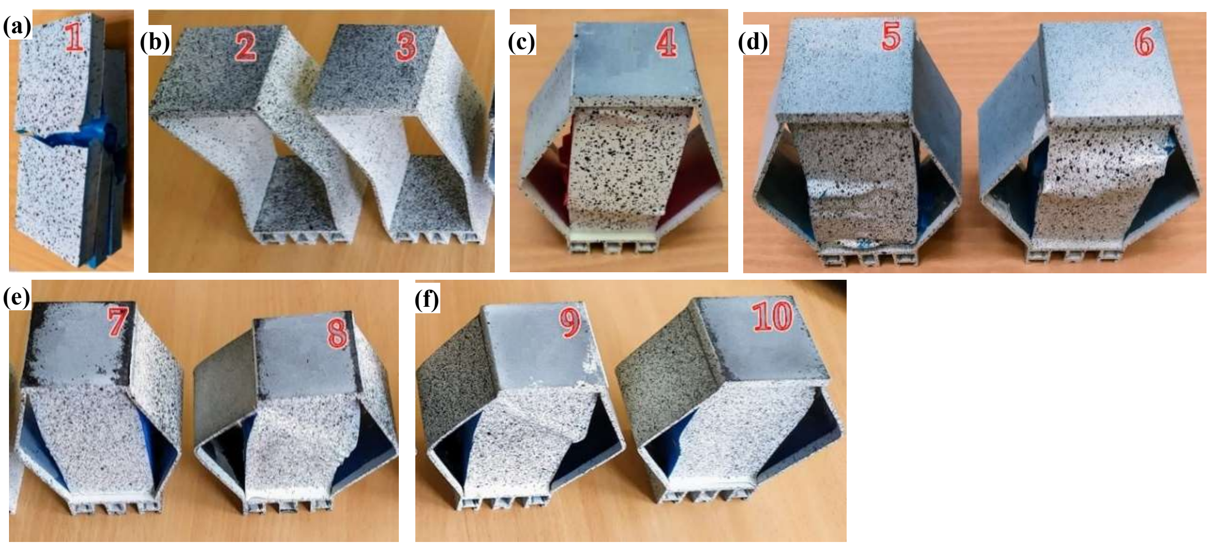

Figure 12. The final deformed shape of the compressive specimens: (a) the printed stiffener "1" having a 10% infill density; (b) the reference fragments "2" and "3" without stiffeners; (c) the sample "4" having a 10% density stiffener without adhesive connection to the profile; (d) to (f) the samples "5" and "6", "7" and "8", and "9" and "10" with 10%, 25%, and 50% density stiffeners glued to profiles.

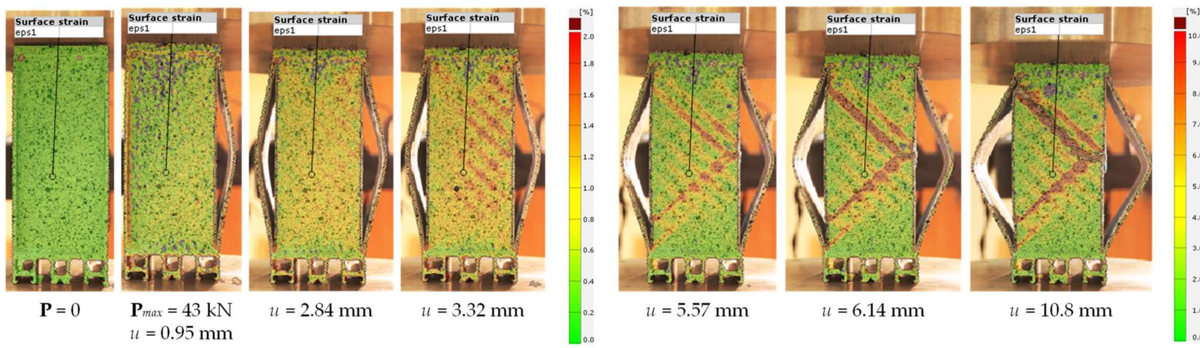

Figure 13. Deformation evolution of the test sample "6" (Fig. 8d) hawing a 10% stiffener adhesively connected to the aluminium profile.

The differences in the shape of the strengthened specimens after the compressive tests are not evident from Figure 12c to Figure 12f. The stiffeners, having the minimum infill density, were suitable to improve the deformation mechanism. That well agree with the results of the sandwich components reported in the literature (Eyvazian et al., 2019). The load-displacement diagrams, shown in Figure 14a, are more informative in this context. The application of the stiffeners adhesively connected to the profile increases the ultimate load more than four times, altering the deformation behaviour of the compressive specimens.

Figure 14b depicts a schematic diagram of the load-resistance components of the profile, having the stiffener with a 10% infill density. The scheme demonstrates that the adhesive bonding of the inserted polymer has a substantial effect on the load resisting at the early deformation stage (the vertical displacements < 1 mm). A considerable scatter of the test results, however, does not allow obtaining a reliable estimation of the resistance of the adhesion contact. The average compressive load corresponding to the loss of the adhesive bond is equal to 43.5 kN; the values 35.7 kN and 49.6 kN define the variation interval of the corresponding load. The ascending branch of the load-deformation diagram of the reference profile adequately determines the location of the characteristic point *A* on Figure 14b. The localisation of the point *B* is a more complex issue because of the substantial variation of both ordinate and abscissa. On the contrary, the infill density of the stiffeners determines the position of the points *C* and *D* adequately. Moreover, the increase in stiffness reduces the scatter of the results.

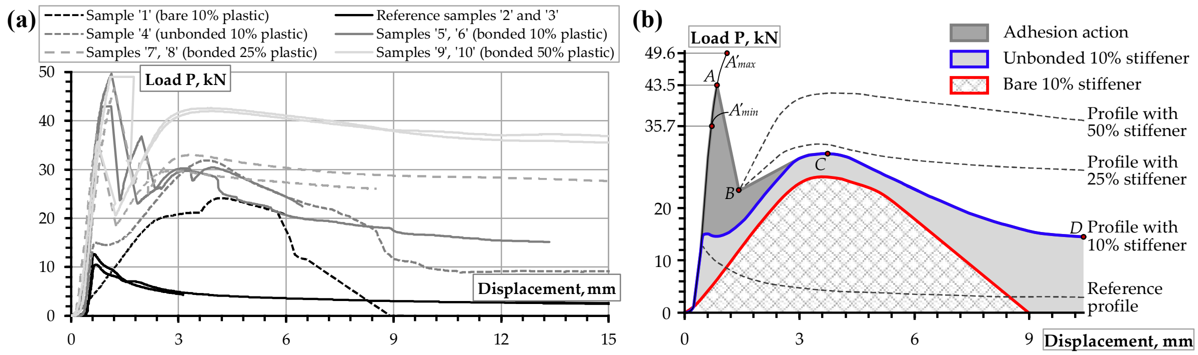

Figure 14. Load-vertical displacement diagrams of the compressive specimens: (a) test results; (b) a schematic diagram of components of the load-resistance mechanism.

3.4 Flexural Tests

The flexural tests employ the same testing apparatus (*H75KS*) and measurement devises (LVDT and DIC), as used in the compressive tests. The loading rate 2.5 mm/min was applied. The parameters and characteristics of the DIC were identical to the compressive tests. A 100 kN load-cell monitored the applied load. The LVDT devices were placed at the mid-span, as shown in Figure 5a. Figure 15 shows the test setup and load-displacement diagrams of the profiles.

The load-displacement diagrams (Figure 15b) show almost doubled load-bearing capacity of the strengthened profiles. The vertical displacements *u* were measured at the mid-span as shown in Figure 5. The average increase in the load-bearing capacity was equal to 1.63; the average increase in deformations corresponding to the ultimate resistance was 2.50, 3.26 and 2.05 times in the profiles with 10%, 25%, and 50% stiffeners, respectively.

Moreover, the stiffened specimens demonstrated the load-bearing resistance exceeding the reference value corresponding to the vertical displacement range not lesser than 22.9 mm; the reference displacement was equal to 5.3 mm (Figure 15b).

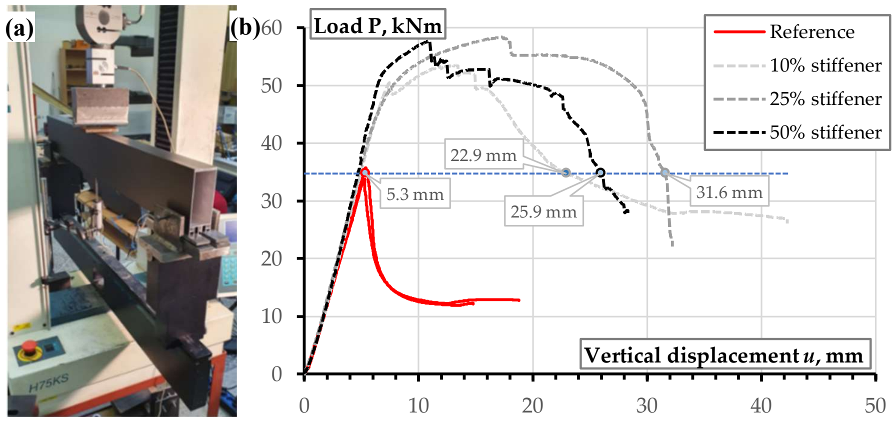

Figure 15. Flexural tests: (a) test apparatus; (b) load-vertical displacement diagrams.

The above results prove the efficiency of the application of low-modulus stiffeners in preventing premature failure of aluminium profiles. The difference in the load-bearing capacity of the strengthened specimens is not significant though failure mechanisms of the beams are different. A local buckling was the test result of the beam strengthened with a 10% infill density stiffener; the breakage of the aluminium web caused the failure of the remaining strengthened profiles. Figure 16 shows the deformed shape of the bending specimens.

As described in the section “Test specimens”, the DIC system was used to identify deformations and failure mechanisms related to the application of the polymeric stiffeners. Figure 17 shows the image correlation results. The generated images correspond to similar loading levels. The differences in the distribution of the deformations of the web are evident. The concentration of the compressive strains causes failure of the profile having stiffeners with a 50% infill density; the reduction of the density of the stiffeners to 25% allows avoiding strain concentration. The failure of the specimen having the stiffener with a 10% infill density is similar to the reference profile though the load-bearing capacity of the strengthened beams remained almost identical (Figure 15b).

The strain distribution maps of Figure 17 ensure a qualitative comparison of deformation mechanisms related to the application of polymeric stiffeners. However, as shown in the references [5] and [45], the DIC approach allows of identifying relative displacements of any points recognised on the exposition surface after the physical tests. Virtual strain gauges created by the *GOM Correlate* software are used for that purpose in this study; 13 virtual indicators, having 20 mm length, were placed on the flat part of the profile web every 10 mm, as shown in Figure 18a. The section near the edge of the strengthening zone was selected to identify the distribution of local strains. Figure 18b–Figure 18e show the strain profiles related to the vertical displacement, *u*.

Figure 16. Deformed shape of the flexural elements: (a) reference specimen; (b)–(d) specimens stiffened respectively with polymeric details having 10%, 25%, and 50% infill density.

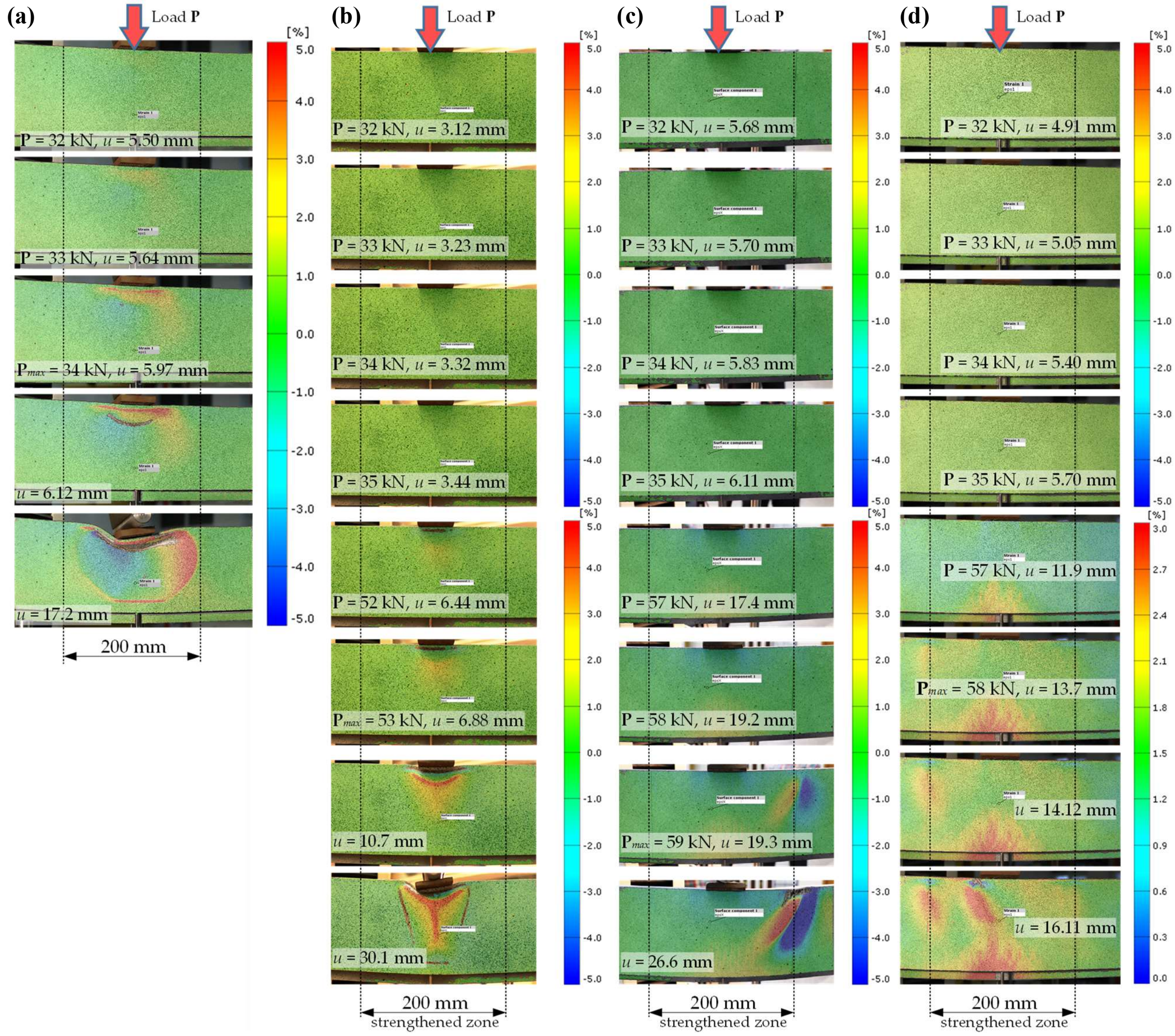

Figure 17. DIC analysis of flexural failure of aluminium profiles: (a) reference specimen; (b)–(d) samples with 10%, 25%, and 50% stiffeners.

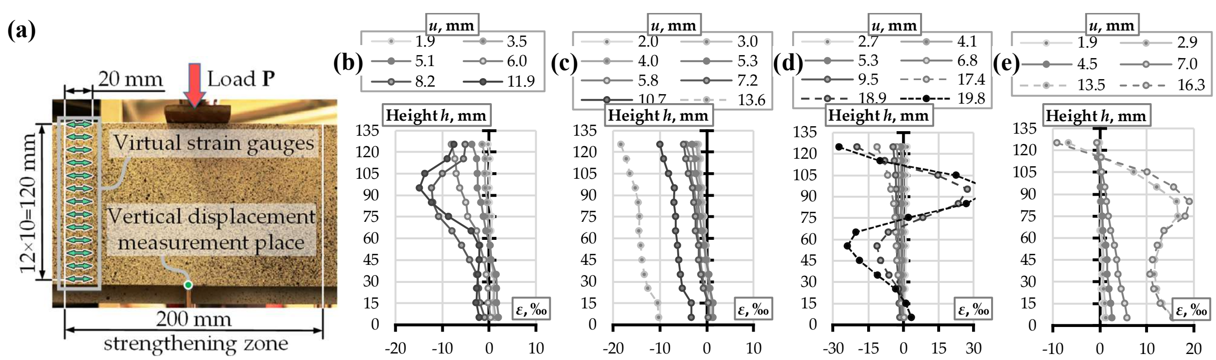

Figure 18. Analysis of the distribution of local strains in the web: (a) virtual strain gauges; (b)–(e) strain profiles of the reference and strengthened specimens with 10%, 25%, and 50% stiffeners.

The strain profiles (Figure 18b–Figure 18e) illustrate non-linearity of local deformations characteristic for both the reference and strengthened profiles. Alteration of the deformations become evident at early loading stages. It is necessary to point out that the above figures show strains estimated at an arbitrarily chosen location. That makes the image correlation technique versatile tool suitable for structural health monitoring purposes. That is well agreeing with findings reported in the literature (Pan et al., 2020; Sharma et al., 2020). The next section presents the results of numerical simulations carried out to evident the deformation mechanisms essential for the adequacy of the structural design.

4. Numerical Simulations

The numerical simulations are carried out to analyse nonlinear effects characteristic of the deformation behaviour of the compression and flexural profiles. The analysis encompasses two stages. Commercial finite element (FE) software SOLIDWORKS 2017 is used to simulate deformation response of the test samples at the first stage. The reference specimens and the profiles strengthened with stiffeners having a 10% infill density are the objects of the analysis. The adequate representation of the ascending branches of the load-deformation diagrams shown in Figure 14a and Figure 15b is the focus of simulations because of the relevance of this behaviour to the structural design problems. The compressive section is the object of the elastic buckling analysis carried out at the second simulation stage. A non-commercial structural analysis software MASTAN2 is used for that purpose.

4.1 Finite Element Simulations of Deformations of Compression and Flexural Profiles

The deformation problems are solved in the 3D formulation, using the Newton-Raphson iteration procedure. Figure 19 shows the corresponding numerical models built up using 3D tetrahedral solid finite elements. A regular mesh with the average size of finite elements of 3 mm was used. Steel plates were modelled to avoid stress concentration at the supports and the load application point. The von Mises material model with bilinear stress-strain diagram is used for aluminium assuming the average experimental values of the modulus of elasticity (E = 70.0 GPa) and the yield strength (f_0 = 228 MPa) of the web-samples (Table 2). The polymeric material was assumed perfectly elastic with modulus E_p=538 MPa. The latter value was determined during the compression test of the bare stiffener (Figure 12a). The SOLIDWORKS software does not ensure modelling the adhesion contact between the inserted polymer stiffener and profile. Therefore, the restricted penetration of the components without bonding adhesion was used in the models of the strengthened specimens.

The boundary conditions were defined to adequately represent the physical test situation (Figure 11 and Figure 15a). Figure 19 shows the support and load conditions. The vertical displacement was applied in small increments (0.3 mm) until the load-bearing capacity was exceeded. The predicted ultimate load of the reference and strengthened specimens was equal to 11.7 kN and 42.3 kN, respectively. That is well agreeing to the test results, when the reference samples resisted the average 11.6 kN ultimate load (Figure 14a); the average resistance of the strengthened specimens was 43.5 kN (Figure 14b).

Figure 20 shows the deformed shape of the simulated profiles subjected to the ultimate compression load. The simulated increase of the ultimate capacity was similar to the test outcomes (Figure 14a): the application of the low-modulus stiffener increases the load-bearing capacity by 3.6 times. The obtained deformed schemes correspond to the test results of Figure 12b and Figure 12d.

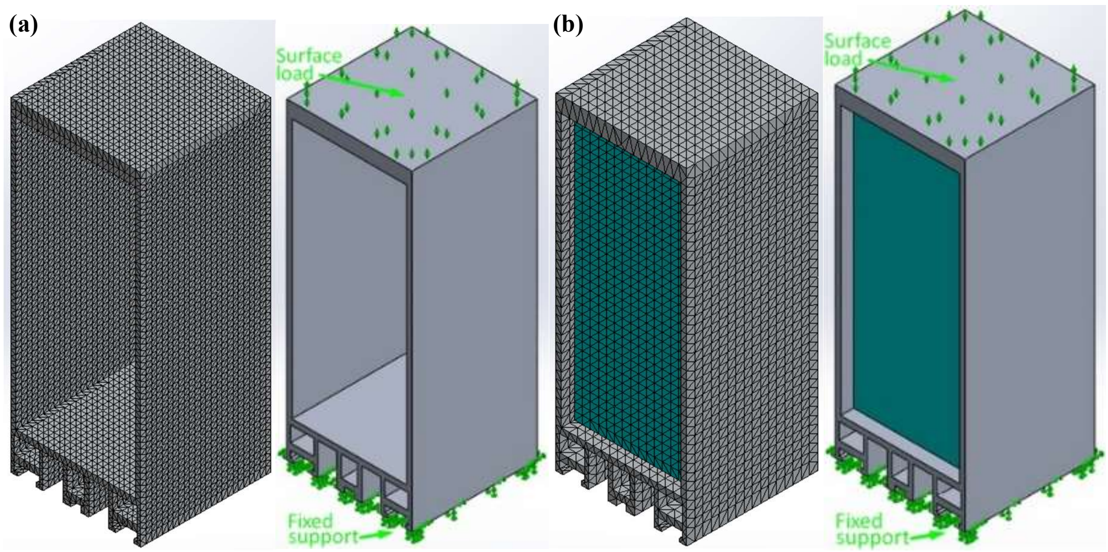

Figure 19. FE mesh and boundary conditions: (a) reference specimen; (b) strengthened profile.

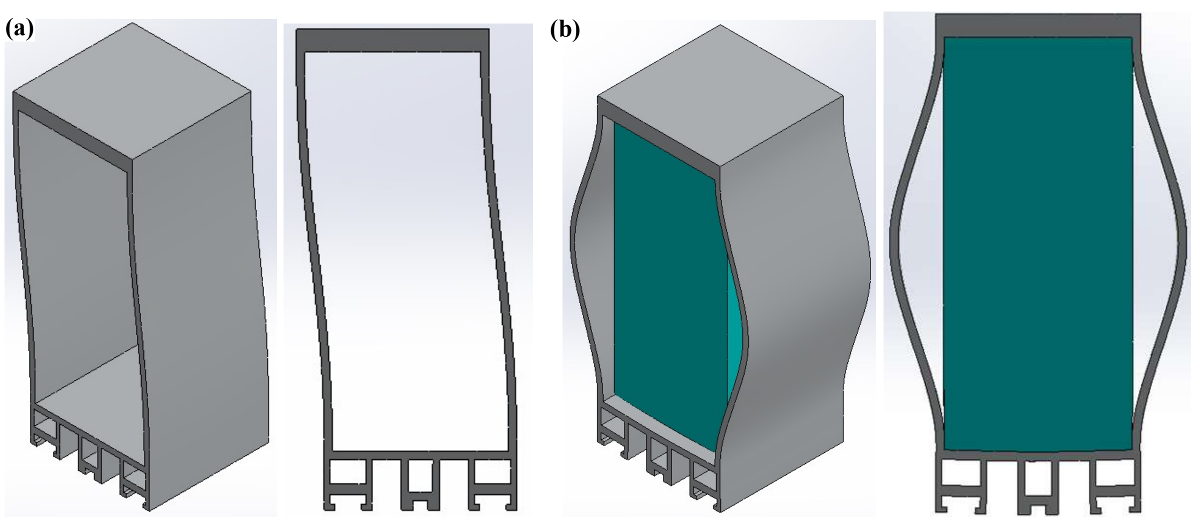

Figure 20. Simulated compression test corresponding to the ultimate compression load: (a) reference specimen (Pmax = 11.7 kN); (b) strengthened profile (Pmax = 42.3 kN).

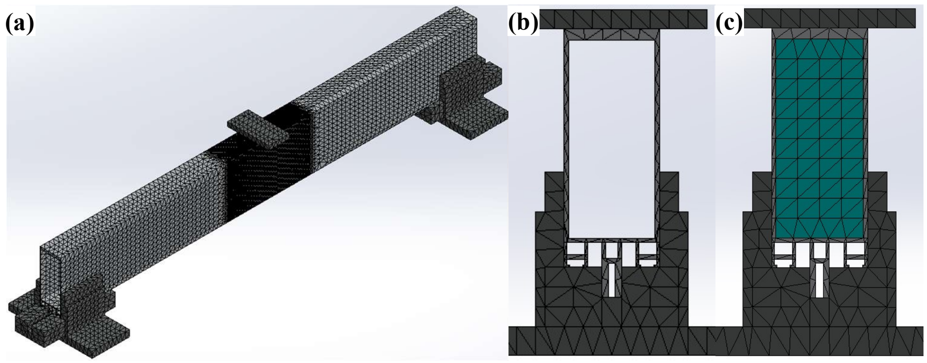

Figure 21. FE mesh of bending specimens: (a) Total view; (b) Support and cross-section of the reference specimen; (c) Support and cross-section of the strengthened profile.

Figure 21 shows the finite element (FE) model of the bending specimens. The similar 3D tetrahedral solid finite elements were used, as for compressive specimens; the same mesh size (3 mm) was used only in the centre part of the beam, corresponding to the strengthened zone (Figure 5a). The remaining parts of the model had an average size of FE mesh equal to 10 mm because of the computer limitations. Figure 22 shows the loading and boundary conditions of the model. The vertical displacement was applied in small increments (0.3 mm) until the load-bearing capacity was exceeded.

Figure 23 demonstrates the load-vertical displacement diagrams of the bending specimens. The noticeable aspect could be related to the overestimation of the actual load-bearing capacity of aluminium profiles. That is a consequence of neglecting non-elastic deformations characteristic of the considered thin-walled structure. The analysis of the strain distribution in the web can help in illustrating those mechanisms.

Figure 24 illustrates the strain distribution in the web, corresponding to the ultimate bending resistance of the FE models. Figure 25 compares the local strain profiles captured by the DIC system and simulated via FE approach. This figure relates the diagrams to the vertical displacement, u. The letter “N” designates the calculation results. Figure 25 shows that the models predict general deformation tendencies, but non-linear effects, appearing at early loading stages (vertical displacement u = 5.8 mm, Figure 25b), are beyond the simulation abilities.

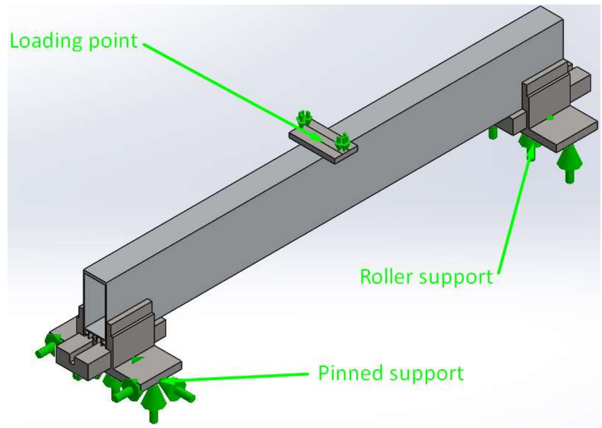

Figure 22. Loading and boundary conditions of FE model of the bending specimen.

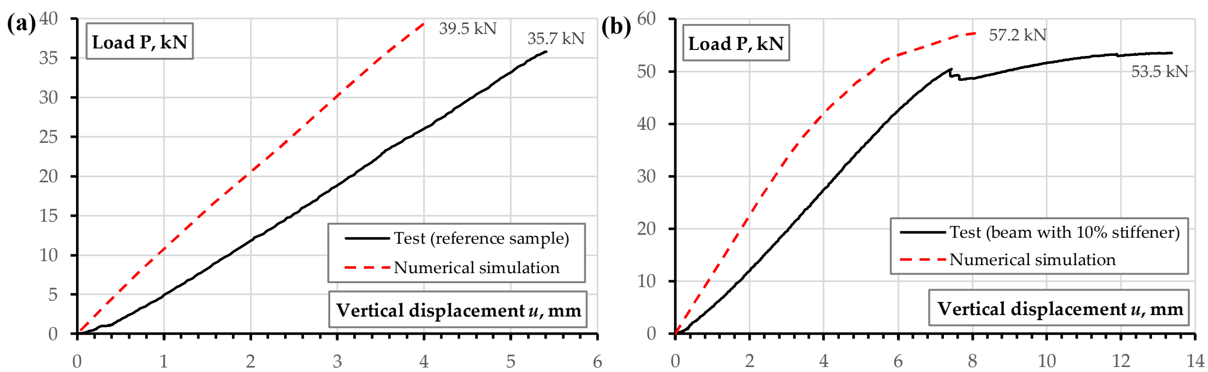

Figure 23. Simulation results of load displacement behaviour of flexural specimens: (a) reference specimen; (b) strengthened profile with the stiffener having a 10% infill density.

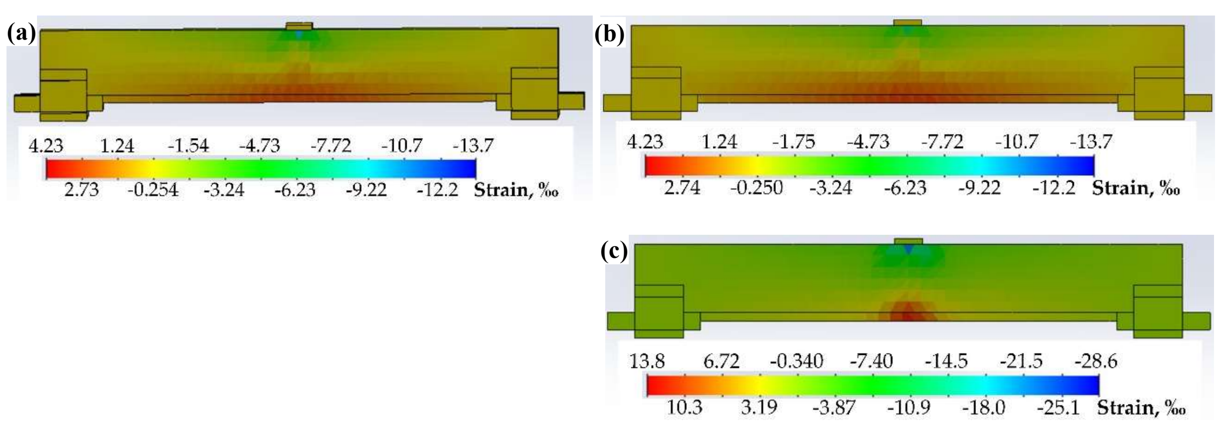

Figure 24. Simulated strain distribution in flexural specimens: (a) reference specimen (vertical displacement u = 3.85 mm); (b) and (c) strengthened profile with the stiffener having a 10% infill density (u = 3.85 mm and 8.06 mm, respectively).

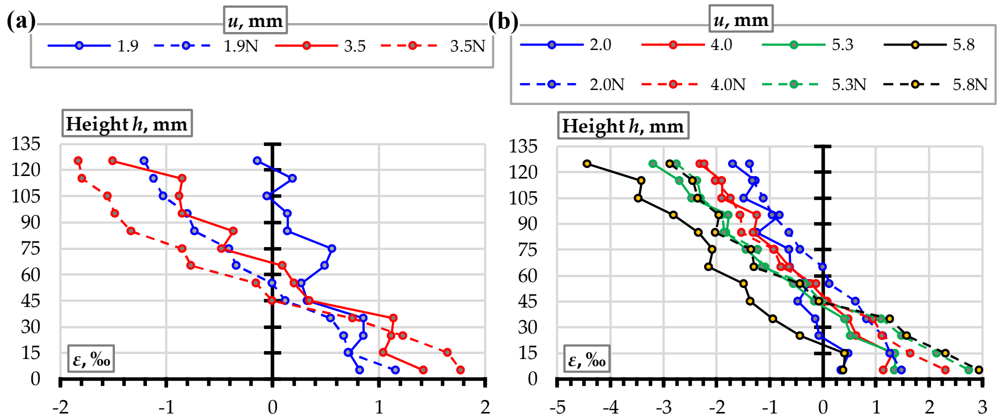

Figure 25. Simulation results of strain distribution in flexural specimens: (a) reference specimen; (b) strengthened profile with the 10% density stiffener.

4.2 Critical Load and Second-Order Elastic Analysis of Compressed Specimens

As can be seen in Figure 12b, the deformed shape of the reference aluminium profile reflects a sway buckling mode. The cross-section parameters (Figure 5b) ensure more than twofold stiffness of the flanges than that of the web. Consequently, the buckling of the web is the predominant failure type. Thus, the elastic buckling of the rigid frame can reflect the failure mechanism of the aluminium sections subjected to compression (section "Compressive tests"). The software MASTAN2 is used to carry out the second-order elastic and critical load analysis.

This software provide the opportunity to perform first- or second-order elastic and inelastic analyses of two- or three-dimensional systems subjected to static load to explain the failure mode of the structural system. Elastic critical load (ECL) analysis of an idealised elastic model of the framed structure determines the shape that the system assumes in the post-critical state in the terms of the eigenvector. This analysis does not include the nonlinear phenomena necessary to determine the magnitude of the ultimate load precisely; it also does not ensure of determining the deformation range, but it adequately predicts the failure manner (Sippel and Blum, 2020). The second-order elastic (SOE) analysis amply represents sway imperfection (also known as *P-Δ effect*) (Zemian and McGuire, 2002). For the solution of nonlinear equilibrium equations, the predictor-corrector and improved polygon method are used (McGuire et al., 2000).

A rectangular frame approximated the aluminium cross-section (Figure 5b); the material properties and dimensions were chosen to retain the actual stiffnesses of the flanges and webs. The bottom corners of the frame were simply supported during the simulations. The reference load $\mathbf{P}_u$ was equal to the ultimate load of the aluminium section at the first buckling mode (Figure 12b). The elastic critical analysis employed the load in a single step; in the second order analysis, the load was applied in small increments (0.01 N) with the maximum number of increments equal to 1000. The applied load ratio (ALR) in comparison to $\mathbf{P}_u$ is analysed further. Figure 26 presents the simulation results.

Figure 26a shows the first buckling mode obtained by elastic buckling analysis at ALR = 1. This failure mode corresponds to the deformed shape of the aluminium section shown in Figure 12b. Figure 26b shows the deformed shape of the frame obtained by second-order elastic analysis, corresponding to ALR = 1, of the initially non-deformed structure. Figure 26c demonstrates the result of the second-order analysis taking into account the influence of the initial sway imperfection of the frame and residual deformation of the components. The first elastic buckling mode of the frame (Figure 26a) described the shape of global and local imperfections. The 1/200 slope of the webs determined the imperfection magnitude. The second-order elastic analysis did not alter the buckling load (ALR = 1), proclaiming the absence of the effects of the deformed geometry (sway imperfection) on the load-bearing capacity of the frame. However, the destabilising influence of initial sway imperfection is evident (comparing to Figure 26b).

Figure 26d shows the first buckling mode from the elastic buckling analysis, corresponding to ALR = 3.84, determined under the assumption of the 1mm lateral displacement of the top flange. The restrain simulated the effect of an adhesive connection between the aluminium profile and stiffener. Figure 13 demonstrates the corresponding experimental tendencies. Figure 26e shows the second buckling mode obtained by elastic buckling analysis, corresponding to ALR = 3.9. The application of an adhesive, jointing the stiffener and aluminium profile, provides sufficient restraint of the web. The experimental specimen fails at ALR≈3.9 (Figure 14). This situation well agrees to the simulated second buckling mode of the rigid frame (Figure 26e).

As shown in Figure 12c, the embedded stiffener without adhesive connection to the profile prevents sway deformations of the frame accentuated by the initial imperfections, and composite section fails in disintegrated buckling mode governed by the symmetric buckling of the webs and share failure of the stiffener. However, Figure 14 shows that overall deformation behaviour and the ultimate resistance failure of the cross-section without an adhesive connection between the constituents is close to the reference fragment. A similar computational result can be obtained verifying structural stability of the rigid frame using second-order analysis without imperfections (Figure 26b). Although the deformed shape of the frame in Figure 26b and Figure 26c are deferent, the second-order elastic analysis (Figure 26b) resulted in the same stiffness of the frame. Thus, the buckling load is remaining the same (ALR = 1).

The above results ensure to relate the effect of the adhesive stiffeners to the alteration of the deformation shape of the cross-section. This solution allowed doubling the load-bearing resistance of the aluminium profiles (mullions). It also can help to avoid imperfection effects during the construction process. The additive manufacturing technology applied to the production of the stiffeners enabled varying the printing density and internal structure of the 3D objects. That makes it a promising tool for the efficient utilisation of construction materials. The obtained results, however, proclaim the primary effect of the adhesive connection of the constituents on the buckling resistance of the hybrid system. This outcome well agrees with the results reported in the literature (Zhao and Zhang, 2007; Fernando et al., 2009; Schnerch, 2005; Islam and Young, 2011; Islam and Young, 2012). Thus, the development of a reliable adhesive connection between the aluminium profile and stiffeners should be the object of further research.

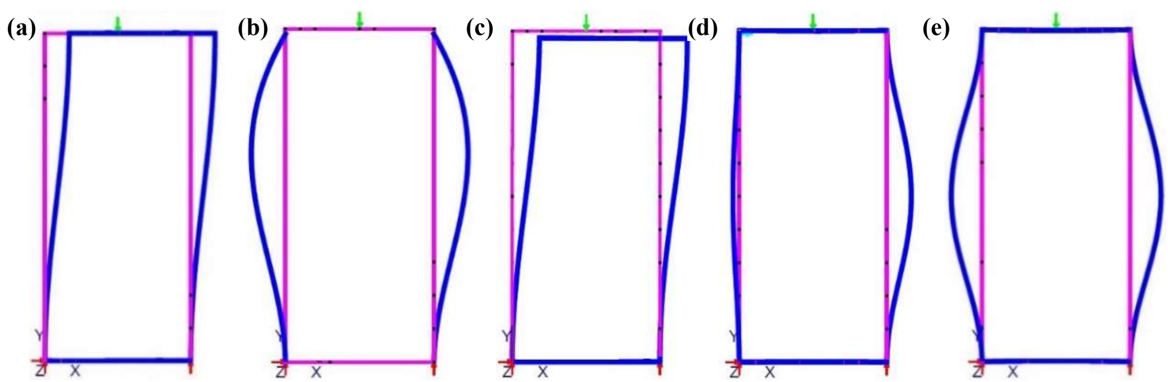

Figure 26. Analysis of compressed specimens: (a) first buckling mode of elastic critical load (ECL), applied load ratio (ALR) = 1; (b) second-order elastic (SOE) without imperfection, ALR = 1; (c) SOE with imperfection (1/200 slope of the webs), ALR = 1; (d) ECL with restrain (1 mm lateral displacement of the flange), ALR = 3.84; (e) Second buckling mode of ECL, ALR = 3.90.

Conclusions

The six-point bending tests were carried out to determine the efficiency of strengthening techniques typical for facade building industry. During these tests local buckling mechanism was detected and further study concentrated on eliminating the premature loss of flexural stiffness. The efficiency of low-modulus stiffeners improving load-bearing capacity of aluminium profiles (mullions) is the object of this research. Polymer stiffeners produced using a 3D printing technique strengthened samples for compression and flexural tests. The infill density of the printed stiffeners was the variable of the study. Numerical simulations were carried out to analyse nonlinear web crippling effects characteristic of the deformation behaviour of the profiles. The following conclusions are formulated from the obtained results:

The application of the low-modulus stiffeners, even of the minimum printing density (with elastic modulus of ≈ 0.54 GPa), adhesively connected to the profiles, doubled the flexural resistance of the specimens. Breakage of the aluminium was the consequence of the tests of the strengthened samples, indicating an efficient utilisation of materials.

The compression tests demonstrated that the application of the low-modulus stiffeners increases the ultimate load more than four times, altering the deformation behaviour of the specimens. The adhesive bonding of the inserted polymer has a substantial effect on the load resisting at the early deformation stage (< 1 mm). A considerable scatter of the test results, however, does not allow obtaining a reliable estimation of the load-bearing capacity. The average compressive load corresponding to the loss of the adhesive bond was equal to 43.5 kN; the values 35.7 kN and 49.6 kN defined the load variation interval. The ascending branch of the load-deformation diagram of the reference (unstrengthen) profile adequately determines the deformation corresponding to the ultimate load. On the contrary, the infill density of the stiffeners determines the shape of the descending branch of the load-deformation diagram; the increase in stiffness (from a 10% printing density through 25% to 50% infill) reduced the scatter of the results.

A perfect agreement between test data of tensile specimens cut from 5.8 mm flange and 2.1 mm web of the profiles is characteristic of ultimate strength. The corresponding average difference between the results is equal to 0.1%. The differences in the yielding limit and the elastic modulus increase to 2.0% and 10.3%, respectively. The later difference demonstrates the potential vulnerability of the thin web to deformation localisation. It is also essential for the adequacy of the finite element modelling.

The results of the elastic critical load analysis well agree to the test outcomes. That put a solid background for the design of composite cross-sections. The results of the tests and numerical simulations also allow relating the effect of the adhesive stiffeners to the alteration of the deformation shape of the cross-section, doubling the load-bearing resistance of the aluminium profiles. The local strengthening can be useful to minimise the effects of the imperfection of the construction process. Thus, the development of a reliable adhesive connection between the aluminium profile and polymeric stiffeners should be the object of further research.

References

Althammer, F.; Ruf, F.; Middendorf, P. Size optimization methods to approximate equivalent mechanical behaviour in thermoplastics. *Journal of Computational Design and Engineering* **2020**, *qwaa069*, 1–19.

Bates, S.R.; Farrow, I.R.; Trask, R.S. 3D printed polyurethane honeycombs for repeated tailored energy absorption. *Materials and Design* **2016**, *112*, 172–183.

Bock, M.; Theofanous, M.; Dirar, S.; Lipitkas, N. Aluminium SHS and RHS subjected to biaxial bending: Experimental testing, modelling and design recommendations. *Engineering Structures* **2021**, *227*, ID: 111468, 1–12.

Ceruti, A.; Marzocca, P.; Liverani, A.; Bil, C. Maintenance in aeronautics in an Industry 4.0 context: The role of Augmented Reality and Additive Manufacturing. *Journal of Computational Design and Engineering* **2019**, *6*, 516–526.

Chen, Y.; Chen, X.; Wang, C. Aluminium tubular sections subjected to web crippling. *Thin-Walled Structures* **2015**, *90*, 49–60.

Chen, Y.; Ye, L.; Escobedo-Diaz, J.P.; Zhang, Y.X.; Fu, K.K. Quasi-static and dynamic progressive crushing of CF/EP composite sandwich panels under in-plane localized compressive loads. *Composite Structures* **2019**, *222*, Paper ID: 110839.

Das, A.; Chatham, C.A.; Fallon, J.J.; Zawaski, C.E.; Gilmer, E.L.; Williams, C.B.; Bortner, M.J. Current understanding and challenges in high temperature additive manufacturing of engineering thermoplastic polymers. *Additive Manufacturing*, **2020,** 34, ID: 101218, 1–21.

Djama, K.; Michel, L.; Gabor, A.; Ferrier, E. Mechanical behavior of a sandwich panel composed of hybrid skins and novel glass fibre reinforced polymer truss core. *Composite Structures* **2019**, *215*, 35–48.

Eyvazian, A.; Taghizadeh, S.A.; Hamouda, A.M.; Tarlochan, F.; Moeinifard, M.; Gobbi, M. Buckling and crushing behavior of foam-core hybrid composite sandwich columns under quasi-static edgewise compression. *Journal of Sandwich Structures and Materials* **2019**, *0*, 1–28, DOI: 10.1177/1099636219894665.

Fernando, D.; Yu, T.; Teng, J.G.; Zhao, X.L. CFRP strengthening of rectangular steel tubes subjected to end bearing loads: Effect of adhesive properties and finite element modelling. *Thin-Walled Structures* **2009**, *47*(10), 1020–1028.

Gao, X.; Zhang, M.; Huang, Y.; Sang, L.; Hou, W. Experimental and numerical investigation of thermoplastic honeycomb sandwich structures under bending loading. *Thin-Walled Structures* **2020,** *155*, Paper ID: 106961, 1–14.

Gribniak, V.; Arnautov, A. K.; Rimkus, A. Development of an anchorage prototype for CFRP stress-ribbon systems using 3D printing technique. In Proceedings of the 13th International Conference *Modern Building Materials, Structures and Techniques*, Vilnius, Lithuania, 16-17 May 2019; VGTU Press: Vilnius, Lithuania, **2019**, 324–328.

Hongshuai, L.; Yao, K.; Wen, I.; Zhou, H.; Fang, D. Experimental and numerical investigation on the crushing behavior of sandwich composite under edgewise compression loading. *Composites Part B* **2016,** *94*, 34–44.

Hou, S.; Li, T.; Jia, Z.; Wang, L. Mechanical properties of sandwich composites with 3d-printed auxetic and non-auxetic lattice cores under low velocity impact. *Materials and Design* **2018**, *160*, 1305–1321.

Islam, S.M.Z.; Young, B. Design of CFRP-strengthened aluminium alloy tubular sections subjected to web crippling. *Thin-Walled Structures* **2018**, *124*, 605–621.

Islam, S.M.Z.; Young, B. FRP strengthened aluminium tubular sections subjected to web crippling. *Thin-Walled Structures* **2011**, *49*(11), 1392–1403.

Islam, S.M.Z.; Young, B. Web crippling of aluminium tubular structural members strengthened by CFRP. *Thin-Walled Structures* **2012**, *59*, 58–69.

Lee, A.D.; Shepherd, P.; Evernden, M.C.; Metcalfe, D. Optimizing the architectural layouts and technical specifications of curtain walls to minimize use of aluminium. *Structures* **2018**, *13*, 8–25.

Lee, A.D.; Shepherd, P.; Evernden, M.C.; Metcalfe, D. Optimizing the cross-sectional shapes of extruded aluminium structural members for unitized curtain wall facades. *Structures* **2017**, *10*, 147–156.

Leśniak, A.; Górka, M. Structural analysis of factors influencing the costs of facade system implementation. *Applied Sciences* **2020**, *10*, Paper ID: 6021.

Li, T.; Wang, L. Bending behavior of sandwich composite structures with tunable 3D-printed core materials. *Composite Structures* **2017**, *175*, 46-57.

Lu, C.; Qi, M.; Islam, S.; Chen, P.; Gao, S.; Xu, Y.; Yang, X. Mechanical performance of 3D-printing plastic honeycomb sandwich structure. *International Journal of Precision Engineering and Manufacturing-Green Technology* **2018**, *5*(1), 47–54.

Lubombo, C.; Huneault, M. A. Effect of infill patterns on the mechanical performance of lightweight 3D-printed cellular PLA parts. *Materials Today Communications* **2018**, *17*, 214–228.

Mamalis, A.G.; Manolakos, M.B.; Ioannidis, M.B.; Papapostolou, D.P. On the crushing response of composite sandwich panels subjected to edgewise compression: experimental. *Composite Structures* **2005**, *71*(2), 246–257.

McGuire, W.; Gallagher, R. H.; Ziemian, R. D. *Matrix Structural Analysis*, Second ed.; Wiley, New York, 2000; pp. 480.

Misiunaite, I.; Gribniak, V.; Rimkus, A.; Jakubovskis, R. The efficiency of utilisation of high-strength steel in tubular profiles. *Materials* **2020**, *13*(5), Paper ID: 1193.

Misiunaite, I.; Rimkus, A.; Jakubovskis, R.; Sokolov, A.; Gribniak, V. Analysis of local deformation effects in cold-formed tubular profiles subjected to bending. *Journal of Constructional Steel Research* **2019**, *160*, 598–612.

Ngo, T. D.; Kashani, A.; Imbalzano, G.; Nguyen, K. T.; Hui, D. Additive manufacturing (3D printing): A review of materials, methods, applications and challenges. *Composites Part B: Engineering* **2018**, *143*, 172–196.

Pan, X.; Yang, T.Y. Post-disaster imaged-based damage detection and repair cost estimation of reinforced concrete buildings using dual convolutional neural networks. *Computer-Aided Civil and Infrastructure Engineering* **2020**, *35*(5), 495–510.

Sarvestani, H. Y.; Akbarzadeh, A.H.; Niknam, H.; Hermenean, K. 3D printed architected polymeric sandwich panels: Energy absorption and structural performance. *Composite Structures* **2018**, *200*, 886–909.

Schneider, C.; Velea, M.N.; Kazemahvazi, S.; Zenkert, D. Compression properties of novel thermoplastic carbon fibre and poly-ethylene terephthalate fibre composite lattice structures. *Materials and Design* **2015,** *65*, 1110–1120.

Schnerch, D. Strengthening of steel structures with high modulus carbon fiber reinforced polymer (CFRP) materials. Ph.D. Thesis, (NC). North Carolina State University, 2005.

Sewell, J.; Czarnecki, T.; Pflug, J. Continuous thermoplastic honeycomb sandwich panel process technology for cost optimal lightweight composites. *Reinforced Plastics*, **2016,** *60*(3), 146–150.

Sharma, G.; Sharma, S.; Sharma, S.Kr. Monitoring structural behaviour of concrete beams reinforced with steel and GFRP bars using acoustic emission and digital image correlation techniques. *Structure and Infrastructure Engineering* **2020**, DOI: 10.1080/15732479.2020.1836661.

Shi, Y.; Liu, W.Q.; Fang, H. Damage characteristics analysis of GFRP-Balsa sandwich beams under Four-point fatigue bending. *Composites Part A: Applied Science and Manufacturing* **2019**, *109*, 564–577.

Shkundalova, O.; Rimkus, A.; Gribniak, V. Structural application of 3D printing technologies: mechanical properties of printed polymeric materials. *Science–Future of Lithuania* **2018**, *10*, Paper ID: mla.2018.6250, 1–8.

Sippel, E.J.; Blum, H.B. System analysis of nonsymmetric cold-formed steel cross sections members. In Proceedings of the Cold-Formed Steel Research Consortium Online Colloquium 51, 20-21 October **2020**, 1–8.

Sivaprakasam, T.; Kesawan, S.; Mahendran, M.; Stringfellow, J.; Baleshan, B. Full-scale tests of aluminium mullion couples in unitized facades under wind actions. *Engineering Structures* **2020**, *215*, Paper ID: 110653.

Taghizadeh, S.A.; Farrokhabadi, A.; Liaghat, Gh.; Pedram, E.; Malekinejad, H.; Mohammadi, S.F.; Ahmadi, H. Characterization of compressive behavior of PVC foam infilled composite sandwich panels with different corrugated core shapes. *Thin-Walled Structures* **2019**, *135*, 160–172.

Waddar, S.; Pitchaimani, J.; Doddamani, M.; Barbero, E. Buckling and vibration behavior of syntactic foam core sandwich beam with natural fiber composite facings under axial compressive loads. *Composites Part B: Engineering*, **2019,** *175*, Paper ID: 107133, 1–11.

Wang, J.; Afshan, S.; Gkantou, M.; Theofanous, M.; Baniotopoulos, C.; Gardner, L. Flexural behaviour of hot-finished high strength steel square and rectangular hollow sections. *Journal of Constructional Steel Research* **2016**, *121*, 97–109.

Wang, Y.Q.; Wang, Z.X.; Yin, F.X.; Yang, L.; Shi, Y.J.; Yin, J. Experimental study and finite element analysis on the local buckling behavior of aluminium alloy beams under concentrated loads. *Thin-Walled Structures* **2016**, *105*, 44–56.

Wu, C.; Zhao, X.L.; Duan, W.H.; Design rules for web crippling of CFRP strengthened aluminium rectangular hollow sections. *Thin-Walled Structures* **2011**, *49*(10), 1195–1207.

Xiao, Y.; Hu, Y.; Zhang, J.; Song, C.; Liu, Z.; Yu, J. Dynamic bending response of CFRP thin-walled square beams filled with aluminum honeycomb. *Thin-Walled Structures* **2018,** *132*, 494–503.

Zaharia, S.M.; Enescu, L.A.; Pop, M.A. Mechanical performances of lightweight sandwich structures produced by material extrusion-based additive manufacturing. *Polymers* **2020**, *12*(8), Paper ID: 1740, 1–19.

Zhang, Y.; Liu, T.; Tizani, W. Experimental and numerical analysis of dynamic compressive response of Nomex honeycombs. *Composites Part B: Engineering* **2018,** *148*, 27–39.

Zhao, X.L.; Zhang, L. State-of-the-art review on FRP strengthened steel structures. *Engineering Structures* **2007**, *29*(8), 1808–1823.

Zhou, F.; Young, B. Aluminium tubular sections subjected to web crippling – Part I: Tests and finite element analysis. *Thin-Walled Structures* **2008**, *46*(4), 339–351.

Zhou, F.; Young, B. Aluminium tubular sections subjected to web crippling – Part II: Proposed design equations. *Thin-Walled Structures* **2008**, *46*(4), 352–361.

Ziemian, R.D.; McGuire, W. Modified Tangent Modulus Approach, a contribution to plastic hinge analysis. *ASCE Journal of Structural Engineering* **2002**, *128*(10), 1301–1307.